Published in final edited form as:
Biomacromolecules. 2012 September 10; 13(9): 2781–2792. doi:10.1021/bm300763x.

Kinetically Controlled Nanostructure Formation in Self-Assembled Globular Protein-Polymer Diblock Copolymers

Carla S. Thomas, **Liza Xu**, and **Bradley D. Olsen***
Department of Chemical Engineering, Massachusetts Institute of Technology, 77 Massachusetts Avenue, Cambridge, Massachusetts 02139, United States

Abstract

Aqueous processing of globular protein-polymer diblock copolymers into solid-state materials and subsequent solvent annealing enables kinetic and thermodynamic control of nanostructure formation to produce block copolymer morphologies that maintain a high degree of protein fold and function. Using model diblock copolymers composed of mCherry-b-poly(N-isopropylacrylamide), orthogonal control over solubility of the protein block through changes in pH and the polymer block through changes in temperature is demonstrated during casting and solvent annealing. Hexagonal cylinders, perforated lamellae, lamellae, or hexagonal and disordered micellar phases are observed depending upon the coil fraction of the block copolymer and the kinetic pathway used for self-assembly. Good solvents for the polymer block produce ordered structures reminiscent of coil-coil diblock copolymers, while an unfavorable solvent results in kinetically trapped micellar structures. Decreasing solvent quality for the protein improves long-range ordering, suggesting that the strength of protein interactions influences nanostructure formation. Subsequent solvent annealing results in evolution of the nanostructures, with the best ordering and the highest protein function observed when annealing in a good solvent for both blocks. While protein secondary structure was found to be almost entirely preserved for all processing pathways, UV-vis spectroscopy of solid-state films indicates that using a good solvent for the protein block enables up to 70% of the protein to be retained in its functional form.

Keywords

block copolymer; self-assembly; protein-polymer conjugate; mCherry; PNIPAM

Introduction

Proteins are poised to enable large advances in future materials through their incorporation into a variety of bioelectronic and biocatalytic devices,[1] pharmaceuticals[2], fuel cells[3] and photovoltaics.[4] Enzymes contribute many favorable qualities to such materials, including large activity, high selectivity, and the ability to operate on unusual substrates. The

*bdolsen@mit.edu.

Supporting Information Available. GPC traces, protein gels, SANS data fitting, UV-vis spectra, FTIR spectra, and analysis of FTIR and CD data to quantitatively determine protein secondary structure. This material is available free of charge *via* the Internet at http://pubs.acs.org.

construction of functional materials often requires large enzyme loading densities, necessitating the use of three-dimensional patterning or immobilization techniques.[5] To date, protein patterning has been accomplished through a wide variety of methods including layer-by-layer assemblies,[6] monolayer films,[7] and the use of lithographic,[8] polymer,[9] and inorganic[10–11] templates. Continued challenges with protein denaturation during incorporation, protein stability within a material, and control over protein nanostructure make the development of new materials central to the improvement of biocatalytic devices.[12]

Self-assembly provides a single-step approach to protein patterning where the native and specific interactions present in proteins can be harnessed to build complex structures over large areas.[13–14] Protein-based materials capable of self-assembly may be created through site-specific bioconjugation to form a protein-polymer diblock copolymer. A variety of bioconjugation techniques have been successfully implemented including grafting-from,[15–16] grafting-to,[16–17] cofactor reconstitution[18–19] and affinity binding[20–21] approaches. To induce self-assembly, a polymer responsive to temperature, pH or light is often used to produce an amphiphilic block copolymer upon stimulus exposure.[20, 22] These amphiphilic molecules self-assemble into a variety of solution-state morphologies depending on relative block lengths,[23] polymer hydrophobicity,[24] and solution conditions including pH and ionic strength.[25] Many of these structures are thought to be kinetically determined due to the variety of observed morphologies.[23] While bioconjugates with polystyrene form micelles as well as vesicles with a bilayer configuration,[21] conjugates with poly(N-isopropylacrylamide) (PNIPAM) have been observed to form micelles and other large aggregates in solution when the temperature is raised above the lower critical solution temperature (LCST) of the PNIPAM homopolymer causing the polymer to collapse.[18, 26–28] Additionally, protein-lipid conjugates have been shown to self-assemble into lipid membranes,[19] and blends of proteins and surfactants have been shown to form lipid bilayer-like structures.[29]

Fewer studies have explored the self-assembly of globular protein-polymer block copolymer gels or solid-state materials. Synthetic block copolymers can be used to template the self-assembly of the bioconjugate material which selectively partitions to one domain of the synthetic block copolymer.[30–32] Alternatively, protein-polymer diblock copolymers may be directly nanopatterned in the solid state by employing the amphiphilic nature of the bioconjugate to induce self-assembly into block copolymer-like nanostructures when solid materials are cast from aqueous solution.[33] This method for patterning protein-based catalysts potentially enables extremely high densities of functional proteins, control over protein orientation, and engineering multiphase transport through different block copolymer nanodomains.

Block copolymer self-assembly directly from solution often results in structures with little long-range ordering,[34] necessitating an annealing step to obtain high quality patterns.[34–37] Due to the thermal sensitivity of most proteins, solvent annealing is the only general option for improving order in protein-polymer block copolymers. As the solvent swells the sample, the block copolymer mobility increases and the solvent compatibilizes the two blocks resulting in a decrease in unfavorable interactions.[34–35] In fully synthetic block copolymers,

studies show that the greatest enhancement in ordering occurs during very short annealing times, with the effect of annealing diminishing with increased time.[34] Different evaporation conditions using the same solvent can also result in different morphologies,[38] and the use of different solvents can result in a variety of morphologies due to differences in relative block solubilities.[39] Solvent annealing also provides a potential route towards improving protein activity and stability in biofunctional systems by utilizing optimal pH, ionic strength, and buffer type.[22, 40]

Both solution casting and solvent annealing processes used to fabricate solid-state globular protein-polymer diblock copolymer nanostructures inherently involve both thermodynamic and kinetic effects, making the specific processing pathway used to prepare materials critical for both nanostructure formation and maintaining protein function. This study investigates processing pathways used to control nanostructure formation as a function of coil fraction, demonstrating that kinetic effects largely determine the type of nanostructure formed. Model material composed of a red fluorescent protein, mCherryS131C, and a thermoresponsive polymer, PNIPAM forms self-assembled nanostructures through water evaporation from aqueous conjugate solutions, and these structures are subsequently solvent annealed to alter ordering. Two orthogonal variables, temperature and pH, are simultaneously used to control the solvent quality for each block during the casting and annealing processes. Nanostructures from conjugates with three different polymer coil fractions are studied to understand the effect of processing on nanodomain morphology, long-range ordering, protein fold, and protein activity.

Materials and Methods

Synthesis of Protein-Polymer Conjugates

Low polydispersity PNIPAM was synthesized using radical addition-fragmentation chain transfer (RAFT) polymerization with a protected maleimide chain transfer agent (CTA) as described previously.[33] The monomer concentration was held constant at 2.0M and the CTA:azobisisobutyronitrile (AIBN) ratio was held constant at 1:0.5. The ratio between the NIPAM monomer and the CTA was varied between 300 and 1000, and the polymerization was performed at 55 °C for 90 to 180 minutes depending upon the desired polymer molecular weight. After isolation of the polymer by precipitation, the polymer was dried under vacuum and the end-group of the CTA was deprotected at 120 °C under vacuum for 2 hours. The polymer molecular weights and polydispersities were determined by gel permeation chromatography (GPC) using an Agilent 1260 Infinity HPLC with N,N-dimethylformamide (DMF) as the mobile phase. Both a refractive index detector and a Wyatt Mini-Dawn 3-angle static light scattering detector were employed to enable absolute molecular weight determination.

Protein expression of the mutant red fluorescent protein, mCherryS131C, was carried out in Luria Broth and purified following the previously described procedure.[33] Site-specific thiol-maleimide bioconjugation and purification were performed as previously reported with a six-fold molar excess of polymer. Three coil fractions (f_{PNIPAM} = 0.42, 0.53, 0.69) (Table 1) were chosen to span a range of molecular designs which would produce different nanostructured morphologies in a traditional coil-coil block copolymer system. Conjugate

purity was assessed by denaturing (SDS-PAGE) and native protein gels and matrix-assisted laser desorption ionization mass spectroscopy (MALDI-MS). The two lower coil fraction conjugates resulted in higher purities around 98% by mass, while the conjugate with the largest PNIPAM coil fraction was approximately 93% pure, as estimated from SDS-PAGE. Conjugate yield was determined spectrophotometrically using the protein absorption at 280 nm (extinction coefficient of 32,550 $M^{-1}cm^{-1}$). The yield of the purified product depended strongly on the molecular weight of the PNIPAM block, with M_n = 57.3 kg/mol resulting in the lowest yield (16%) while materials with M_n = 18.8 and 29.0 kg/mol were obtained in yields of 31% and 36%, respectively. The decreased yield at higher polymer molecular weight is due primarily to lower yield of the bioconjugation reaction.

Sample Preparation

Conjugate solutions, dialyzed into pure water, were concentrated to ~70 mg/mL using Millipore Ultra-15 centrifugal filters with a molecular weight cutoff of 3 kDa. Conjugate behavior was studied in four different solutions. A protein-selective solvent is achieved using an aqueous solution above the thermal transition of the conjugate materials (40 °C, pH = 7.5). In contrast, a polymer-selective solvent is realized using a solution near the isoelectric point (pI) of the protein (25 °C, pH = 5.7). Additionally, a non-selective solvent is obtained using a room temperature pH = 7.5 solution, and a non-solvent is created with a solution at pH = 5.7 and a temperature of 40 °C. Bulk samples of nanostructured conjugate were created by evaporating the solvent at room temperature or 40 °C. The solvent evaporation rate at room temperature was controlled using a vacuum controller with a ramp rate of 300 Torr/hour and a final setpoint of 75 Torr, while evaporation at 40 °C was performed at ambient pressure. Samples were subsequently solvent vapor annealed at room temperature in either water or a 1 vol% formic acid solution for 8, 24, or 72 hours. The solvent annealing setup consisted of approximately 1 cm of solvent in the bottom of a sealed glass jar with an inverted beaker on which the sample was placed, giving a sample to liquid distance of 4 cm. No appreciable loss of solvent during annealing occurred. After annealing, samples were allowed to dry under ambient conditions (below the glass transition temperature of the material), kinetically arresting the process of structure evolution.

Sample Characterization

Dynamic light scattering (DLS) experiments were performed on a DynaPro Nanostar at a scattering angle of 90° with a laser wavelength of 658 nm. UV-vis spectra were collected using a Cary 50 UV-vis spectrophotometer. A spectrophotometric measure of protein function is calculated as A_{586} of the sample relative to A_{586} of the as-synthesized conjugate, where both values are normalized by A_{280} to control for variation in protein concentration. At least three replicates were averaged for each sample to produce the final data. Circular dichroism (CD) spectra were measured on an Aviv model 202 CD spectrometer operating at 25 °C and background corrected. Spectra were analyzed for secondary structure content with CDPro software using the CONTINLL, SELCON3, and CDSSTR methods. Fourier transform infrared (FTIR) spectroscopy was performed using a Thermo Nexus 870 and analyzed using OMNIC software. Fourier self-deconvolutions (FSD) of the amide I peak were performed using a bandwidth of 30 cm^{-1} and an enhancement factor of 2.5 for general secondary structural identification.[41–42]

Small-angle neutron scattering (SANS) experiments were performed on the Low-Q Diffractometer (LQD) end station at Los Alamos Neutron Science Center (LANSCE). Hydrogenated conjugate samples were dialyzed into 98% deuterated water and loaded into a quartz cell. Absolute intensities were obtained by correcting for background scattering and open beam neutron flux. The resulting spectra were fit with either the Beaucage[43] model or the Percus-Yevick[44–45] model depending on the solvent quality for the polymer block. For the Percus-Yevick model, effects of polydispersity and Gaussian smearing were taken into consideration. SANS experiments were repeated at both 1 wt% and 3 wt%, producing quantitatively identical results. Small-angle X-ray scattering (SAXS) and transmission electron microscopy (TEM) samples approximately 1 mm in thickness were cast on Kapton tape using 1 mm thick anodized aluminum washers as a mold. SAXS experiments were performed on beamline X9 of the National Synchrotron Light Source (NSLS) at Brookhaven National Lab, and the data was corrected for empty cell and dark field scattering. The scattering from several replicates of similar materials were measured to ensure reproducibility of nanostructure formation, and acquisition times were chosen such that the effect of beam damage on sample nanostructure was undetectable. Bulk samples were cryo-microtomed using a Leica EM UC6 at −110 °C to a thickness of 60 nm, and stained with ruthenium tetroxide vapors from a 0.5 % aqueous solution for 20 minutes. This treatment preferentially stains the protein domains, making them appear darker in images. A JEOL 2000FX TEM was used to obtain bright field images using an accelerating voltage of 120 kV and a LaB_6 filament. Images were captured using an ORCA camera in a fixed bottom mount configuration.

Results and Discussion

Characterization of Solution Nanostructure

The solution-state processing pathway used to self-assemble solid-state nanomaterials has a large impact on the final material structure due to the potential for nanostructures formed in solution to be kinetically trapped in the final solid-state material. DLS and SANS are used to assess the aggregation state of the globular protein-polymer block copolymers in solution, providing insight into the initial structure during processing for different solvent conditions. While DLS provides information about the size of conjugate aggregates in solution, SANS allows the nanostructure within the aggregates to be studied. Table 2 shows both average particle sizes and measured polydispersities obtained by DLS as a function of solvent quality and coil fraction. The average hydrodynamic radii measured in non-selective and polymer-selective solvents increase with increasing PNIPAM coil fraction and the values are consistent with individual molecules of protein-polymer conjugate. Based on the protein length of 4.2 nm from the crystal structure[46] (PDB 2H5Q) and the root mean square end-to-end distance of PNIPAM with a Kuhn segment length of 0.7 nm,[47] calculated values of 6.6, 7.7, and 10.0 nm are obtained for the three PNIPAM coil fractions of 0.42, 0.53, and 0.69, respectively. These calculations assume a dumbbell configuration for the conjugate which is consistent with previous experimental observations on protein-PEG conjugates.[48] As expected, the calculations using an ideal polymer chain model slightly underestimate the experimental measurement, which is performed in a good solvent for the polymer.

SANS experiments, as illustrated in Figure 1, show similar results for the non-selective and polymer-selective solvents with no signs of aggregation. Curves for samples in a good solvent for the polymer were fit with a Beaucage[43] model which was selected for its ability to fit the form factor of the protein-polymer conjugate without prior knowledge of the polymer configuration around the protein. At $f_{PNIPAM} = 0.53$, fits give an effective radius of gyration (R_g) for the conjugate of 7.5 ± 1.4 and 6.9 ± 1.2 nm for non-selective and polymer-selective solvents, respectively. For the conjugate with $f_{PNIPAM} = 0.69$, the R_g increased to 15.0 ± 3.8 and 18.0 ± 5.5 nm in the non-selective and polymer-selective solvents, respectively, in agreement with the hydrodynamic radii obtained by DLS. For the smaller conjugate with a coil fraction of 0.42, the R_g was measured to be 11.8 ± 2.9 and 10.2 ± 2.8 nm in the non-selective and polymer-selective solvents, respectively. These molecular sizes are similar within measurement error to the conjugate with 53% PNIPAM and to the size measured by DLS. The terminal behavior at high q is characterized by power law exponentials of 1.36 ± 0.01, 1.62 ± 0.02, and 1.41 ± 0.01 for the three PNIPAM coil fractions in order of increasing coil fraction. As expected, the power law exponents are only weakly dependent on the solvent quality for the protein block, and they are intermediate between a Gaussian coil and an ideal rod and close to that expected for a coil in a good solvent.

In poor solvents for the polymer block, large-scale aggregation occurs, as indicated by an apparent particle radius in excess of 800 nm by DLS. After several hours, a macrophase separated precipitate is clearly observable by eye, and SANS patterns show a peak characteristic of ordering in the aggregated phase. Fitting with a Percus-Yevick model[44–45] for disordered hard spheres gives hard sphere radii of 14.5 ± 0.2, 17.9 ± 0.2, and 21.2 ± 0.3 nm for increasing PNIPAM coil fractions. These results are consistent with the formation of collapsed PNIPAM domains above the thermal transition temperature, followed by phase separation of the aggregated conjugates to form nanostructured phases. SANS observes the short length scale ordering within macrophase separated regions, while DLS predominantly detects the large scale size of the macrosphase separated aggregates.

Unlike traditional block copolymers where micelles or vesicles are observed in a selective solvent for either block,[49] these globular protein-polymer block copolymers show phase behavior that is dominated by the behavior of the polymer block. Near the pI of the protein and below the LCST of the PNIPAM homopolymer where the solvent is selective for the polymer, the block copolymers remain soluble in their monomeric form. It is important to note that monomer formation under these conditions may only be observed for proteins with relatively high solubilities such as mCherry, and that it may not be generalizable to all proteins. At elevated temperatures, where the solvent is selective for the protein, the block copolymers macrophase separate from solution regardless of the solvent quality for the protein. This behavior suggests that the protein block in the corona has insufficient electrostatic and entropic repulsive interactions to form stable aggregated structures.

Kinetically-Determined Structure Formation

As diblock copolymers are concentrated from dilute solution to induce self-assembly, the solvent quality has a large effect on the type of nanostructure formed due to kinetic effects

on block copolymer self-assembly, as illustrated by SAXS in Figure 2 and TEM in Figure 3. When cast from good solvents for the PNIPAM block, mCherry-PNIPAM19 (f_{PNIPAM} = 0.42) tends to form hexagonal cylinder phases. The SAXS pattern of a sample cast from a non-selective solvent shows broad, overlapping higher order peaks at √3q* and 2q*, indicating a poorly-ordered hexagonal morphology. A TEM image of this sample (Figure 3c) shows PNIPAM cylinders in an mCherry matrix in both end-on and edge-on orientations with very small grain sizes. When the material is cast from a polymer-selective solvent, sharper SAXS peaks are observed at both √3q*and 2q*, indicating an improvement in hexagonal order. Microscopy images (Figure 3a) further verify the presence of larger grains of well-formed PNIPAM cylinders in an mCherry matrix. In contrast, samples prepared from a non-solvent for the polymer block result in a disordered micellar structure. The primary SAXS peak is broader and only a broad shoulder is observable at higher q, indicating a greater degree of disorder than for samples cast from a good solvent for the polymer. A disordered micellar structure is confirmed by TEM, as shown in Figure 3f. In many areas of the disordered micellar sample, the PNIPAM nanodomains encircle or nearly encircle mCherry nanodomains which is surprising because PNIPAM is the minority component.

At a coil fraction of 0.53, mCherry-PNIPAM29 also shows a strong morphology dependence on the polymer selectivity of the solvent. In samples cast from a non-selective solvent, SAXS patterns (Figure 2b) show an asymmetric primary peak with a low q shoulder and multiple overlapping higher order reflections which do not allow clear identification of the nanodomain structure. The patterns look similar to previously observed scattering patterns from hexagonally perforated lamellae in these materials;[33] however, the low q shoulder and higher order peaks are less pronounced. TEM images of the sample cast from a non-selective solvent (Figure 3d) show mCherry structures in a PNIPAM matrix with regions exhibiting both hexagonal and perforated lamellar structures observed. In contrast, TEM images of samples cast from a polymer-selective solvent show a predominately lamellar morphology (Figure 3b) with better ordering than samples cast from a non-selective solvent. However, the X-ray scattering pattern shows little change as compared with the sample cast from a non-selective solvent. When a non-solvent for the polymer block is used to prepare materials, mCherry-PNIPAM29 forms micellar structures composed of discrete mCherry nanodomains surrounded by a continuous PNIPAM nanodomain similar to mCherry-PNIPAM19. Peaks at √3q* and √7q* in the SAXS patterns suggest hexagonal ordering of the nanostructures, and TEM images (Figure 3f) clearly illustrate the micellar structure with hexagonal packing.

At the highest studied PNIPAM fraction (f_{PNIPAM} = 0.69), mCherry-PNIPAM57 self-assembles into highly disordered lamellar morphologies when cast from a good solvent for the polymer, while hexagonal micellar morphologies are formed during casting from a non-solvent for the polymer. SAXS curves of samples cast from a good solvent for the polymer show broad primary peaks with relatively low intensities, typical of disordered structures; however, a weak peak at 2q* is observed indicating some ordering is present. TEM images of a sample cast from a non-selective solvent, illustrated in Figure 3e, show a relatively disordered morphology with very short curved lamellar-like domains similar to morphologies observed in coil-coil block copolymers near the order-disorder transition.[50]

The hexagonal phase formed from poor solvents for the polymer block is characterized by large polymer domains separated by thin protein-rich regions (Figure 3h). These structures are reminiscent of a kinetically-trapped morphology formed by the aggregation of solution nanostructures, and SAXS patterns indicate hexagonal packing of these structures with peaks at √3q* and √7q*.

The combined measurements of structure in solution and in the solid-state suggest that kinetics govern the effect of polymer solvent quality on nanostructure formation according to the pathways for self-assembly illustrated in Figure 4. In a good solvent for the polymer block, conjugates remain as individual molecules in solution until a comparatively high concentration, at which point self-assembly occurs from homogenous solution. This self-assembly pathway results in morphologies that resemble those of traditional block copolymers.[51–52] Cylinders, perforated lamellae, and lamellae are observed in order of increasing coil fraction, although the specific coil fractions at which these three morphologies are observed are higher than in coil-coil diblock copolymers. In contrast, a non-solvent for the polymer block causes aggregation even at low concentrations as the PNIPAM domains collapse, minimizing their interactions with the solvent. PNIPAM aggregation drives macrophase separation from solution, and further concentration of conjugate leads to the enrichment of these macrophase separated domains. This yields nanostructures with hexagonal symmetry due to packing of micellar nanodomains. Unexpectedly, mCherry cores are observed at low PNIPAM fractions and PNIPAM cores are observed at high PNIPAM fractions. It is hypothesized that at low coil fractions, the unstable mCherry coronas collapse to produce inverted micellar domains, while at higher coil fractions, the PNIPAM is kinetically trapped in the micelle core due to the higher penalty for chain diffusion at high molecular weight.

Unlike the large effect of polymer solvent quality, protein solvent quality does not significantly change the kinetic pathway for self-assembly in mCherry-PNIPAM materials. However, minimizing the electrostatic repulsion between mCherry blocks by tuning the pH to be near the pI does improve the quality of order observed, and in the case of mCherry-PNIPAM29, produces a change in the type of nanodomain formed. Although this processing strategy may result in significantly different results depending upon protein solubility and protein-protein interactions near the pI, these results suggest that tuning protein interactions is an important strategy for promoting ordered nanostructure formation. It is hypothesized that polymer solvent quality has a much larger effect than protein solvent quality in this system because of the very large change in PNIPAM solubility over the temperature range explored.

In addition to changes in the nanostructure symmetry, the samples cast from poor solvents for the polymer always produced morphologies with larger domain spacing, and the magnitude of this effect increases as the coil fraction increases. For a coil fraction of 0.42, the domain spacing increases from approximately 21.3 nm for materials cast from a good solvent for the polymer block to 23 nm for materials cast from a non-solvent for the polymer block. At a coil fraction of 0.53, the domain spacing increases from approximately 28 nm to 34 nm, while for a coil fraction of 0.69, the increase is from 36 nm to 44 nm for the same solvent conditions. These observations are consistent with the more strongly-segregated

nature of the protein-selective solvent and non-solvent casting conditions, where unfavorable mixing between PNIPAM and water induces net repulsive interactions between the PNIPAM and the highly soluble mCherry. Due to the unfavorable polymer-solvent interactions, the polymer stretches to minimize interfacial contact and remains kinetically trapped in the strongly-segregated structure in the final solid-state morphology.

Effect of Solvent Annealing on Structure Evolution

Solvent annealing was explored to improve the order of protein-polymer block copolymer nanostructures and to provide insight into kinetic effects in as-cast samples. Non-selective (room temperature water) and polymer-selective (1% formic acid) solvents were used for solvent annealing because poor solvents for the polymer block do not provide the necessary increase in polymer block mobility. Samples cast from a non-selective solvent were solvent annealed in either a non-selective or a polymer-selective solvent, and samples cast from a polymer-selective solvent were annealed in only a non-selective solvent. These conditions provide at least one processing stage using a non-selective solvent and are expected to produce structures with the best ordering closest to that of the equilibrium morphology while simultaneously preserving a large fraction of protein in its functional form.

Depending upon the coil fraction of the mCherry-PNIPAM block copolymer, solvent annealing in a non-selective solvent may result in improved ordering, a change in nanodomain structure, or a decrease in ordering due to the interplay between kinetic effects on structure formation and the thermodynamics of self-assembly. For mCherry-PNIPAM19 (f_{PNIPAM} = 0.42), all solvent annealing conditions lead to improved ordering of hexagonal cylindrical nanostructures after 8 hours, as evidenced by the decreasing width of the primary peak and more clearly resolved peaks at $\sqrt{3}q^*$ and $2q^*$ (Figure 5a–c). Samples cast from a polymer-selective solvent and annealed in a non-selective solvent for 24 to 72 hours show continuous improvements in order with increasing annealing time, as evidenced by a continuous sharpening of the primary peak in SAXS and two clearly separate higher order reflections at 72 hours. In contrast, samples cast from a non-selective solvent and annealed in a non-selective solvent for 24 to 72 hours result in a slight increase in the width of the primary SAXS peak and blurring together of the two higher order peaks, as compared to the 8 hour anneal. TEM of the sample annealed for 24 hours (Figure 6a) shows well-formed PNIPAM cylinders embedded in a continuous mCherry matrix with both end-on and side-on grain orientations observed. The common approach to a hexagonal cylinder phase for all materials annealed in a non-selective solvent suggests that this phase is thermodynamically favorable for mCherry-PNIPAM19. While annealing in an acidic solution results in improved ordering up to 8 hours, the 24 and 72 hour annealed samples show a rapidly broadening primary peak and the disappearance of higher order peaks, indicative of an order-disorder transition in the materials. It is hypothesized that an increasing concentration of acid accumulates in the film during annealing, and the accumulated positive charge on the protein promotes disordering of the block copolymer.

Annealing mCherry-PNIPAM29 (f_{PNIPAM} = 0.53) in a non-selective solvent results in an improvement in nanodomain ordering followed by a change in nanodomain structure from hexagonal or perforated lamellar to lamellar (Figure 5d–f). Similar structural changes are

observed from samples originally cast from a non-selective or a protein-selective solvent. After 8 hours of annealing in a non-selective solvent, higher order peaks become more distinct, indicating a higher degree of ordering. The domain spacing does not change appreciably after this short annealing time. After 24 hours of annealing a sample cast from a polymer-selective solvent, large perforated lamellar grains with polymer domains clearly perforating protein domains are observable by TEM (Figure 6b). Despite the observation of larger perforated lamellar grains in TEM at 24 hours, SAXS patterns show growth of the 001 and 002 peaks and diminishing intensity of the 100 shoulder and 200 reflection, suggesting that a transition to a lamellar phase has started. Annealing for 72 hours provides sufficient chain mobility for the nanostructures to rearrange to lamellae (Figure 6c), suggesting that the perforated lamellar morphology is kinetically trapped. When the sample is cast from a non-selective solvent and annealed for 24 hours in a non-selective solvent, this transition to a more lamellar structure has already begun, and few indications of perforated lamellar or hexagonal ordering remain (Figure 6d). When a sample cast from a non-selective solvent is instead annealed for 24 hours in a polymer-selective solvent, protein perforations of polymer domains are still observed (Figure 6e). As with mCherry-PNIPAM19, annealing in a polymer-selective solvent shows a rapid increase in disorder with increasing annealing time, resulting in loss of order for annealing times longer than 24 hours. Solvent annealing results in an increase in domain spacing of 10–20% due to solvent swelling after 72 hours for all three conditions.

In contrast to smaller coil fractions where solvent annealing improves ordering, for mCherry-PNIPAM57 ($f_{PNIPAM} = 0.69$) the degree of ordering decreases slightly with increasing solvent annealing time, as evidenced by the decreasing intensity of the primary scattering peak. The relatively high coil fraction is anticipated to decrease the water concentration required to reach the order-disorder transition, promoting a slight loss of order with increasing swelling. SAXS (Figure 5g–i) shows that the primary peak intensity decreases, particularly from 24 to 72 hours of annealing for all samples. In addition, the second order peak intensity decreases, with the most prominent decrease occurring after acidic solvent anneals. For all three annealing conditions, the domain spacing increases with increasing annealing time from 36 nm to 40–45 nm as the polymer swells with water. A TEM image of this sample cast from a non-selective solvent and then annealed in the same solvent for 24 hours (Figure 6f) shows a highly disordered lamellae-like nanostructure, similar to that seen in the non-annealed sample. These results suggest that mCherry-PNIPAM57 is relatively close to the order-disorder transition, and that added solvent during annealing results in an increase in disorder due to compatibilization of the two blocks.

The complex effect of solvent annealing on structure formation reflects the interplay of kinetic and thermodynamic driving forces governing structure formation during solvent annealing. While the addition of a non-selective solvent increases chain mobility and promotes relaxation towards an equilibrium morphology, it also changes the thermodynamic equilibrium by introducing an additional component into the block copolymer system that swells the nanodomain structure. In the case of mCherry-PNIPAM19, chain mobility effects dominate, as evidenced by a very minor change in domain spacing with increasing annealing time, and enhanced ordering is observed. In the case of mCherry-PNIPAM57, a 30% increase in domain spacing leads to a decrease in ordering without a change in

nanostructure, indicating that swelling effects dominate. For mCherry-PNIPAM29, both structural rearrangement and changes in domain spacing are observed. The interplay between structure evolution and increased swelling with increased annealing time yields a range of optimal annealing times from 8 to 24 hours where enhanced long-range ordering is observed without a large degree of nanodomain swelling.

In contrast to behavior during annealing with non-selective solvents, annealing with a dilute acid (polymer-selective solvent) leads to a more rapid loss of order. Unlike pH-controlled casting solutions where the formic acid molarity is constant, the film is an open system in contact with a chemical potential bath during solvent annealing. Therefore, significant formic acid is absorbed into the nanostructures during annealing, as evidenced by a change in the color of the materials from dark red to gold due to protonation of the mCherry acylimine group.[53–54] Protonation of mCherry induces a net positive charge that increases electrostatic repulsions between molecules and promotes disordering within the nanostructures. This is consistent with the observation that casting from solutions with a pH near the pI (minimizing electrostatic interactions) enhances ordering.

Protein Structure and Function

Molecular design and the processing conditions used to induce self-assembly have a large effect on the function of the protein in the solid-state. Solid-state UV-vis provides a measure of the protein function in the bulk self-assembled material, allowing its dependence on casting and annealing conditions to be quantified. In mCherry, the chromophore is sensitive to the surrounding environment, making UV-vis absorption an excellent indicator for the maintenance of protein fold and function. Figure 7a shows that for all PNIPAM coil fractions, casting from a non-selective solvent preserved the highest levels of protein function, with up to 70% of the original solution-state absorbance preserved. Samples cast from acidic solutions show a relative decrease in absorbance at 586 nm which corresponds to the appearance of a new peak at 440 nm, indicative of a spectral shift due to protonation of the acylimine chromopohore.[53–56] Therefore, UV-vis measurements for acid-cast samples underestimate the fraction of functional protein in the solid state. The amount of functionality preserved also depends on coil fraction. For samples cast at room temperature protein function decreases weakly with increasing coil fraction, while for samples cast from a non-solvent the chromophore absorbance peak increases weakly with increasing coil fraction. The variation in protein function with changing coil fraction may be due to a combination of compositional and morphological effects which cannot be clearly differentiated due to the relationship between block copolymer composition and morphology.

Comparison between solid-state and rehydrated solution absorption measurements provides a method to separate functionality losses due to irreversible denaturation from losses due to spectral shifts caused by association in the solid-state or protonation of the mCherry chromophore by residual acid. For all conditions, the rehydrated absorbance is lower than the as-synthesized conjugate, indicating an irreversible loss of functionality ranging from 5 to 45%, as shown in Figure 7b. However, the level of retained functionality is higher than in the solid-state, clearly indicating that part of the decrease in absorbance in the solid-state is

reversible and not due to protein unfolding and chromophore degradation. Casting from a good solvent for the polymer block results in higher reconstituted protein function than casting from a poor solvent for the polymer for all coil fractions. Surprisingly, casting from an acidic solution also led to much higher activity levels after rehydration than casting from a neutral pH solution. This suggests that the decreased functionality observed for acid-cast samples is primarily due to protonation of the chromophore, and that the addition of the small molecule actually has a functionality-preserving effect. The preserving effect is speculated to be due to hydrogen bonding with residual formate ions in the film that may stabilize the protein in a manner similar to that of pharmaceutical additives.[57]

Solvent annealing may also have an impact on the function of the protein within nanostructured materials. Annealing water-cast samples in pure water does not significantly alter protein function, but for samples which become significantly swollen like mCherry-PNIPAM57, the protein chromophore absorbance increases with annealing time by approximately 20% of the original solution value (Figure S7). This is consistent with the effect of protein rehydration to increase absorbance. However, when annealing at an acidic pH, the fast drop in A_{586} indicates that chromophore protonation occurs rapidly and is nearly complete within 8 hours. In contrast, annealing with water after casting samples at acidic pH leads to a more gradual increase in A_{586} with longer annealing times as residual acid is slowly released from the film. It is also observed that there is a wide degree of variability between the samples cast from an acidic solution and annealed in a non-selective solvent. Regardless of the rate of increase in A_{586}, the A_{440} inversely tracks with A_{586}, consistent with variability due to inhomogeneous acid diffusion out of the film. Measurements on rehydrated protein after solvent annealing indicate that the annealing time does not greatly affect the fraction of folded protein when annealing in a non-selective solvent. For those samples annealed in an acidic solution, it is observed that a short anneal results in a small initial decrease in overall functionality (4–12% of original absorbance) due to chromophore protonation, after which there is negligible loss of functionality with increased annealing time. Regardless of annealing condition, the lowest coil fraction always retains the highest level of protein function in samples rehydrated after annealing.

The secondary structure of the protein was assessed in both self-assembled nanostructures and rehydrated conjugates, showing that despite changes in protein function with processing, the secondary structure is largely preserved. Using FTIR spectra, the secondary structure is determined from the amide I region between 1600 and 1700 cm^{-1} using a Fourier self-deconvolution algorithm.[41–42, 58–60] As shown in Figures S8–10, the amide I peak shows no resolvable change with different processing conditions for a given PNIPAM coil fraction. Figure 8 provides representative spectra for each conjugate along with the corresponding deconvolutions which show that the primary difference among the conjugates is the enhancement of the deconvoluted peak centered around 1650 cm^{-1} with increasing coil fraction. The five peaks obtained upon deconvolution were attributed to secondary structures in accordance with the literature (Table 3).[41–42, 58–63] The peak at 1631 cm^{-1} is the most intense for coil fractions of 0.42 and 0.53, which is consistent with a predominately β-sheet protein. At $f_{PNIPAM} = 0.42$ approximately 43% of the conjugate was β-sheet structures, while at $f_{PNIPAM} = 0.53$ this value was 40%. For the conjugate with a coil fraction of 0.69, the amide I peak maximum is shifted to 1649 cm^{-1}, indicative of a larger random coil

fraction, and the β-sheet fraction was reduced to 38%. As expected, a decrease in the relative β-sheet content was observed at the larger PNIPAM coil fractions due to the increasing polymer coil fraction of the material. However, the observed decrease is smaller than predicted based on the increasing coil fraction alone (see Supporting Information), which suggests that conjugates with a higher polymer coil fraction have a slightly higher β-sheet content in the protein. Circular dichroism (CD) measurements on rehydrated conjugate confirm the preservation of secondary structure after self-assembly. The spectra for each rehydrated conjugate are indistinguishable from the as-synthesized conjugate, showing predominantly β-sheet structure with the same β-sheet content as the corresponding as-synthesized conjugate (Table S5–7).

While protein secondary structure retention is required to maintain high levels of protein functionality, changes in tertiary structure also contribute to overall protein function. Even though secondary structure remained largely unaltered, displaying a high fraction of β-sheet content as expected from the mCherry crystal structure,[46] the chromophore absorbance of mCherry was found to be dependent on charge state and slightly dependent on processing time and bioconjugate coil fraction. This suggests that the tertiary structure of some fraction of the protein is disrupted during self-assembly, resulting in an irreversible loss of function ranging from 5 to 45% of the total protein. However, several processing conditions are identified that appear to maintain 80–95% of the protein in its folded form.

Conclusions

Model globular protein-polymer block copolymers composed of an mCherry protein block and a PNIPAM polymer block are shown to self-assemble into cylinders, perforated lamellae, lamellae, or hexagonal and disordered micellar phases depending on both the polymer coil fraction and the solvent quality for each block. Temperature modulation during self-assembly alters the solvent quality and consequently the morphology; a good solvent for the polymer produces nanostructures reminiscent of coil-coil block copolymers. When a poor solvent for the polymer block is used, aggregates that form in solution are kinetically trapped in the solid-state to form disordered micellar structures. Tuning protein interactions also affects nanostructure formation, as samples cast from solutions near the isoelectric point of the protein where repulsive interactions between proteins are minimized produce nanostructures with improved ordering. At the smallest polymer coil fraction studied ($f_{PNIPAM} = 0.42$), a hexagonal morphology is strongly preferred. However, at the largest coil fraction ($f_{PNIPAM} = 0.69$), disordered lamellae are observed which may indicate that these samples are near an order-disorder transition. Bioconjugates with an intermediate coil fraction ($f_{PNIPAM} = 0.53$) result in several morphologies including perforated lamellae and lamellae depending on the processing history, demonstrating the importance of kinetic effects on structure control. Solvent annealing materials with $f_{PNIPAM} = 0.53$ results in a trend towards lamellar nanostructure under many conditions. As the coil fraction in the block copolymer is increased, solvent annealing for 8–24 hours in a non-selective solvent is shown to enhance the quality of nanostructures ($f_{PNIPAM} = 0.42$), change the morphology ($f_{PNIPAM} = 0.53$), or simply swell existing nanodomains ($f_{PNIPAM} = 0.69$).

Depending upon the block copolymer coil fraction and processing technique used to induce self-assembly, a large fraction of the protein function could be preserved in the solid state. Using a neutral pH solution, up to 70% of the initial protein function is maintained when in a solid film with the highest retention observed at the lowest coil fraction. In contrast, using an acidic solution results in a spectral shift due to chromophore protonation which is reversed upon rehydration to recover up to 95% of the original protein function. Despite variations in protein function, the secondary structure remains intact regardless of the processing conditions used in this study. Overall, these results indicate that a large majority of the protein tertiary structure can be preserved in self-assembled materials.

Supplementary Material

Refer to Web version on PubMed Central for supplementary material.

Acknowledgments

This research was supported by the Department of Energy Office of Basic Energy Sciences (award number DE-SC0007106). SANS experiments were performed on the LQD at the Los Alamos Neutron Science Center. SAXS experiments were performed at Beamline X9 at the National Synchrotron Light Source at Brookhaven National Laboratory, and TEM experiments were performed at the MIT Institute for Soldier Nanotechnology. CD and DLS experiments were performed at the Biophysical Instrumentation Facility for the Study of Complex Macromolecular Systems (NSF-0070319 and NIH GM68762). We also thank Rex Hielm for experimental assistance with SANS, and Lin Yang for experimental assistance with SAXS.

References

1. Willner I, Katz E. Integration of Layered Redox Proteins and Conductive Supports for Bioelectronic Applications. Angew Chem, Int Ed. 2000; 39:1180–1218.
2. Patel RN. Synthesis of Chiral Pharmaceutical Intermediates by Biocatalysis. Coord Chem Rev. 2008; 252:659–701.
3. Reda T, Plugge CM, Abram NJ, Hirst J. Reversible Interconversion of Carbon Dioxide and Formate by an Electroactive Enzyme. Proc Natl Acad Sci U S A. 2008; 105:10654–10658. [PubMed: 18667702]
4. Das R, Kiley PJ, Segal M, Norville J, Yu AA, Wang LY, Trammell SA, Reddick LE, Kumar R, Stellacci F, Lebedev N, Schnur J, Bruce BD, Zhang SG, Baldo M. Integration of Photosynthetic Protein Molecular Complexes in Solid-State Electronic Devices. Nano Lett. 2004; 4:1079–1083.
5. Ge J, Lu DN, Liu ZX, Liu Z. Recent Advances in Nanostructured Biocatalysts. Biochem Eng J. 2009; 44:53–59.
6. Wang Y, Angelatos AS, Caruso F. Template Synthesis of Nanostructured Materials *via* Layer-by-Layer Assembly. Chem Mater. 2008; 20:848–858.
7. Kumashiro Y, Ikezoe Y, Tamada K, Hara M. Dynamic Interfacial Properties of Poly(ethylene glycol)-Modified Ferritin at the Solid/Liquid Interface. J Phys Chem B. 2008; 112:8291–8297. [PubMed: 18570392]
8. Kim DC, Sohn JI, Zhou DJ, Duke TAJ, Kang DJ. Controlled Assembly for Well-Defined 3D Bioarchitecture Using Two Active Enzymes. ACS Nano. 2010; 4:1580–1586. [PubMed: 20180558]
9. Laible PD, Kelley RF, Wasielewski MR, Firestone MA. Electron-Transfer Dynamics of Photosynthetic Reaction Centers in Thermoresponsive Soft Materials. J Phys Chem B. 2005; 109:23679–23686. [PubMed: 16375348]
10. Luo G, Zhang Q, Castillo ARD, Urban V, O'Neill H. Characterization of Sol-Gel-Encapsulated Proteins Using Small-Angle Neutron Scattering. ACS Appl Mater Interfaces. 2009; 1:2262–2268. [PubMed: 20355861]

11. Vinoba M, Lim KS, Lee SH, Jeong SK, Alagar M. Immobilization of Human Carbonic Anhydrase on Gold Nanoparticles Assembled onto Amine/Thiol-Functionalized Mesoporous SBA-15 for Biomimetic Sequestration of CO_2. Langmuir. 2011; 27:6227–6234. [PubMed: 21488617]
12. Rodrigues RC, Berenguer-Murcia A, Fernandez-Lafuente R. Coupling Chemical Modification and Immobilization to Improve the Catalytic Performance of Enzymes. Adv Synth Catal. 2011; 353:2216–2238.
13. Dutta, NK.; Choudhury, NR. Self-Assembly and Supramolecular Assembly in Nanophase Separated Polymers and Thin Films. Springer; New York: 2008. p. 220-304.
14. Sear RP. Interactions in Protein Solutions. Curr Opin Colloid Interface Sci. 2006; 11:35–39.
15. Heredia KL, Bontempo D, Ly T, Byers JT, Halstenberg S, Maynard HD. *In Situ* Preparation of Protein - "Smart" Polymer Conjugates with Retention of Bioactivity. J Am Chem Soc. 2005; 127:16955–16960. [PubMed: 16316241]
16. van Hest JCM. Biosynthetic-Synthetic Polymer Conjugates. Polym Rev. 2007; 47:63–92.
17. Kalia J, Raines RT. Advances in Bioconjugation. Curr Org Chem. 2010; 14:138–147. [PubMed: 20622973]
18. Wan XJ, Liu SY. Fabrication of a Thermoresponsive Biohybrid Double Hydrophilic Block Copolymer by a Cofactor Reconstitution Approach. Macromol Rapid Commun. 2010; 31:2070–2076. [PubMed: 21567633]
19. Hamachi I, Nakamura K, Fujita A, Kunitake T. Anisotropic Incorporation of Lipid-Anchored Myoglobin into a Phospholipid Bilayer Membrane. J Am Chem Soc. 1993; 115:4966–4970.
20. Boyer C, Huang X, Whittaker MR, Bulmus V, Davis TP. An Overview of Protein-Polymer Particles. Soft Matter. 2011; 7:1599–1614.
21. Cho HY, Kadir MA, Kim BS, Han HS, Nagasundarapandian S, Kim YR, Ko SB, Lee SG, Paik HJ. Synthesis of Well-Defined (Nitrilotriacetic Acid)-End-Functionalized Polystyrenes and Their Bioconjugation with Histidine-Tagged Green Fluorescent Proteins. Macromolecules. 2011; 44:4672–4680.
22. Shakya AK, Sami H, Srivastava A, Kumar A. Stability of Responsive Polymer-Protein Bioconjugates. Prog Polym Sci. 2010; 35:459–486.
23. Reynhout IC, Cornelissen JLM, Nolte RJM. Self-Assembled Architectures from Biohybrid Triblock Copolymers. J Am Chem Soc. 2007; 129:2327–2332. [PubMed: 17274615]
24. Reynhout IC, Cornelissen JLM, Nolte RJM. Synthesis of Polymer-Biohybrids: From Small to Giant Surfactants. Acc Chem Res. 2009; 42:681–692. [PubMed: 19385643]
25. van Rijn P, Böker A. Bionanoparticles and Hybrid Materials: Tailored Structural Properties, Self-Assembly, Materials and Developments in the Field. J Mater Chem. 2011; 21:16735–16747.
26. Mougin NC, van Rijn P, Park H, Müller AHE, Böker A. Hybrid Capsules *via* Self-Assembly of Thermoresponsive and Interfacially Active Bionanoparticle-Polymer Conjugates. Adv Funct Mater. 2011; 21:2470–2476.
27. Li M, De P, Li H, Sumerlin BS. Conjugation of RAFT-Generated Polymers to Proteins by Two Consecutive Thiol-ene Reactions. Polym Chem. 2010; 1:854–859.
28. Kulkarni S, Schilli C, Müller AHE, Hoffman AS, Stayton PS. Reversible Meso-Scale Smart Polymer-Protein Particles of Controlled Sizes. Bioconjugate Chem. 2004; 15:747–753.
29. Nassar AEF, Zhang Z, Chynwat V, Frank HA, Rusling JF, Suga K. Orientation of Myoglobin in Cast Multibilayer Membranes of Amphiphilic Molecules. J Phys Chem. 1995; 99:11013–11017.
30. Presley AD, Chang JJ, Xu T. Directed Co-Assembly of Heme Proteins with Amphiphilic Block Copolymers Toward Functional Biomolecular Materials. Soft Matter. 2011; 7:172–179.
31. Hu YX, Samanta D, Parelkar SS, Hong SW, Wang QA, Russell TP, Emrick T. Ferritin-Polymer Conjugates: Grafting Chemistry and Integration into Nanoscale Assemblies. Adv Funct Mater. 2010; 20:3603–3612.
32. Kim B, Lam CN, Olsen BD. Nanopatterned Protein Films Directed by Ionic Complexation with Water-Soluble Diblock Copolymers. Macromolecules. 2012
33. Thomas CS, Glassman MJ, Olsen BD. Solid-State Nanostructured Materials from Self-Assembly of a Globular Protein-Polymer Diblock Copolymer. ACS Nano. 2011; 5:5697–5707. [PubMed: 21696135]

34. Kim SH, Misner MJ, Xu T, Kimura M, Russell TP. Highly Oriented and Ordered Arrays from Block Copolymers *via* Solvent Evaporation. Adv Mater. 2004; 16:226–231.
35. Cavicchi KA, Berthiaume KJ, Russell TP. Solvent Annealing Thin Films of Poly(isoprene-b-lactide). Polymer. 2005; 46:11635–11639.
36. Segalman RA. Patterning with block copolymer thin films. Mat Sci Eng R. 2005; 48:191–226.
37. Albert JNL, Epps TH. Self-assembly of block copolymer thin films. Mater Today. 2010; 13:24–33.
38. Kim G, Libera M. Morphological Development in Solvent-Cast Polystyrene-Polybutadiene-Polystyrene (SBS) Triblock Copolymer Thin Films. Macromolecules. 1998; 31:2569–2577.
39. Lodge TP, Pudil B, Hanley KJ. The Full Phase Behavior for Block Copolymers in Solvents of Varying Selectivity. Macromolecules. 2002; 35:4707–4717.
40. Saluja A, Kalonia DS. Nature and Consequences of Protein-Protein Interactions in High Protein Concentration Solutions. Int J Pharm. 2008; 358:1–15. [PubMed: 18485634]
41. Byler DM, Susi H. Examination of the Secondary Structure of Proteins by Deconvolved FTIR Spectra. Biopolymers. 1986; 25:469–487. [PubMed: 3697478]
42. Jackson M, Mantsch HH. The Use and Misuse of FTIR Spectroscopy in the Determination of Protein Structure. Crit Rev Biochem Mol Biol. 1995; 30:95–120. [PubMed: 7656562]
43. Beaucage G. Approximations Leading to a Unified Exponential/Power-Law Approach to Small-Angle Scattering. J Appl Crystallogr. 1995; 28:717–728.
44. Kinning DJ, Thomas EL. Hard-Sphere Interactions Between Spherical Domains in Diblock Copolymers. Macromolecules. 1984; 17:1712–1718.
45. Seitz ME, Burghardt WR, Faber KT, Shull KR. Self-Assembly and Stress Relaxation in Acrylic Triblock Copolymer Gels. Macromolecules. 2007; 40:1218–1226.
46. Shu XK, Shaner NC, Yarbrough CA, Tsien RY, Remington SJ. Novel Chromophores and Buried Charges Control Color in mFruits. Biochemistry. 2006; 45:9639–9647. [PubMed: 16893165]
47. Zhang W, Zou S, Wang C, Zhang X. Single Polymer Chain Elongation of Poly(N-isopropylacrylamide) and Poly(acrylamide) by Atomic Force Microscopy. J Phys Chem B. 2000; 104:10258–10264.
48. Pai SS, Hammouda B, Hong K, Pozzo DC, Przybycien TM, Tilton RD. The Conformation of the Poly(ethylene glycol) Chain in Mono-PEGylated Lysozyme and Mono-PEGylated Human Growth Hormone. Bioconjugate Chem. 2011; 22:2317–2323.
49. Hanley KJ, Lodge TP, Huang CI. Phase Behavior of a Block Copolymer in Solvents of Varying Selectivity. Macromolecules. 2000; 33:5918–5931.
50. Sakamoto N, Hashimoto T. Ordering Dynamics of a Symmetric Polystyrene-block-polyisoprene. 2. Real-Space Analysis on the Formation of Lamellar Microdomain. Macromolecules. 1998; 31:3815–3823.
51. Bates FS, Fredrickson GH. Block Copolymers - Designer Soft Materials. Phys Today. 1999; 52:32–38.
52. Park C, Yoon J, Thomas EL. Enabling Nanotechnology with Self Assembled Block Copolymer Patterns. Polymer. 2003; 44:6725–6760.
53. Pakhomov AA, Pletneva NV, Balashova TA, Martynov VI. Structure and Reactivity of the Chromophore of a GFP-like Chromoprotein from *Condylactis gigantea*. Biochemistry. 2006; 45:7256–7264. [PubMed: 16752914]
54. Gross LA, Baird GS, Hoffman RC, Baldridge KK, Tsien RY. The Structure of the Chromophore within DsRed, a Red Fluorescent Protein from Coral. Proc Natl Acad Sci U S A. 2000; 97:11990–11995. [PubMed: 11050230]
55. Subach FV, Malashkevich VN, Zencheck WD, Xiao H, Filonov GS, Almo SC, Verkhusha VV. Photoactivation Mechanism of PAmCherry Based on Crystal Structures of the Protein in the Dark and Fluorescent States. Proc Natl Acad Sci U S A. 2009; 106:21097–21102. [PubMed: 19934036]
56. Bravaya KB, Subach OM, Korovina N, Verkhusha VV, Krylov AI. Insight into the Common Mechanism of the Chromophore Formation in the Red Fluorescent Proteins: The Elusive Blue Intermediate Revealed. J Am Chem Soc. 2012; 134:2807–2814. [PubMed: 22239269]

57. Kamerzell TJ, Esfandiary R, Joshi SB, Middaugh CR, Volkin DB. Protein-Excipient Interactions: Mechanisms and Biophysical Characterization Applied to Protein Formulation Development. Adv Drug Deliv Rev. 2011; 63:1118–1159. [PubMed: 21855584]
58. Kong J, Yu S. Fourier Transform Infrared Spectroscopic Analysis of Protein Secondary Structures. Acta Biochim Biophys Sin. 2007; 39:549–559. [PubMed: 17687489]
59. Fu K, Griebenow K, Hsieh L, Klibanov AM, Robert L. FTIR Characterization of the Secondary Structure of Proteins Encapsulated within PLGA Microspheres. J Controlled Release. 1999; 58:357–366.
60. Herberhold H, Marchal S, Lange R, Scheyhing CH, Vogel RF, Winter R. Characterization of the Pressure-induced Intermediate and Unfolded State of Red-shifted Green Fluorescent Protein—A Static and Kinetic FTIR, UV/VIS and Fluorescence Spectroscopy Study. J Mol Biol. 2003; 330:1153–1164. [PubMed: 12860135]
61. Barth A, Zscherp C. What Vibrations Tell Us About Proteins. Q Rev Biophys. 2002; 35:369–430. [PubMed: 12621861]
62. Huang W, Krishnaji S, Hu X, Kaplan D, Cebe P. Heat Capacity of Spider Silk-Like Block Copolymers. Macromolecules. 2011; 44:5299–5309. [PubMed: 23869111]
63. Matheus S, Friess W, Mahler HC. FTIR and nDSC as Analytical Tools for High-Concentration Protein Formulations. Pharm Res. 2006; 23:1350–1363. [PubMed: 16715365]

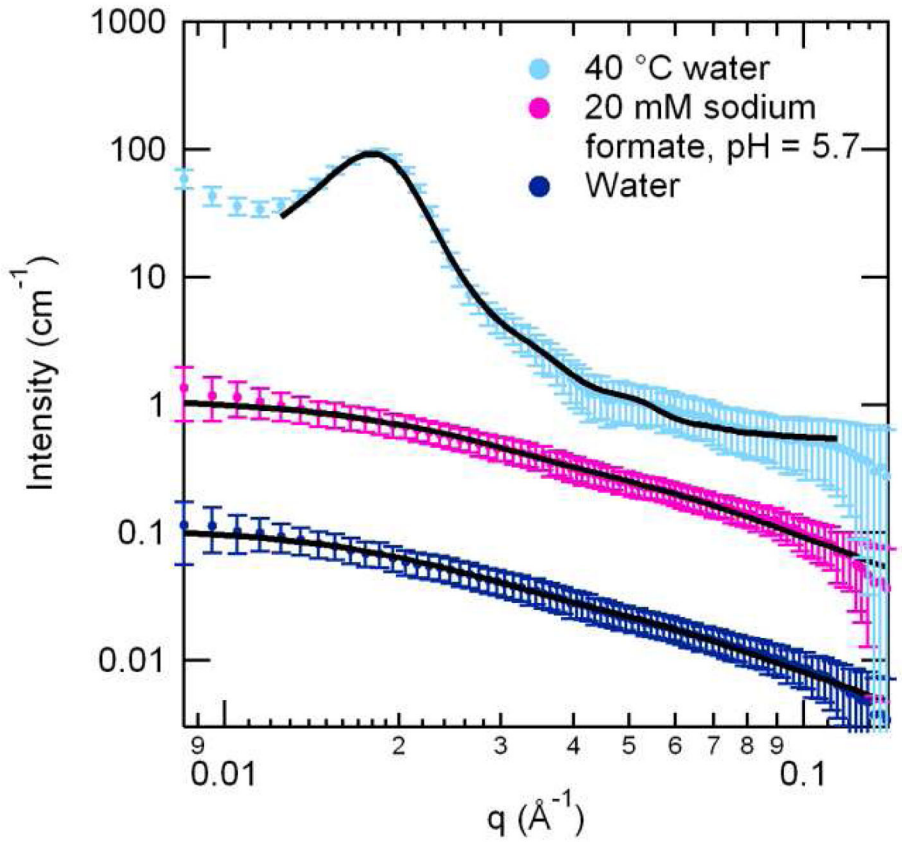

Figure 1.

Small-angle neutron scattering patterns of a 3 wt% solution of mCherry-PNIPAM29 (f_{PNIPAM} = 0.53). Solid lines show fits to the data. Non-selective (room temperature, neutral pH) and polymer-selective (room temperature, pH 5.7) solvents contain conjugates in the monomeric state, while samples in a protein-selective solvent (40 °C, neutral pH) result in aggregation. The 20 mM sodium formate pH = 5.7 and 40 °C water traces have been vertically offset by 10 and 100 cm^{-1}, respectively, for clarity.

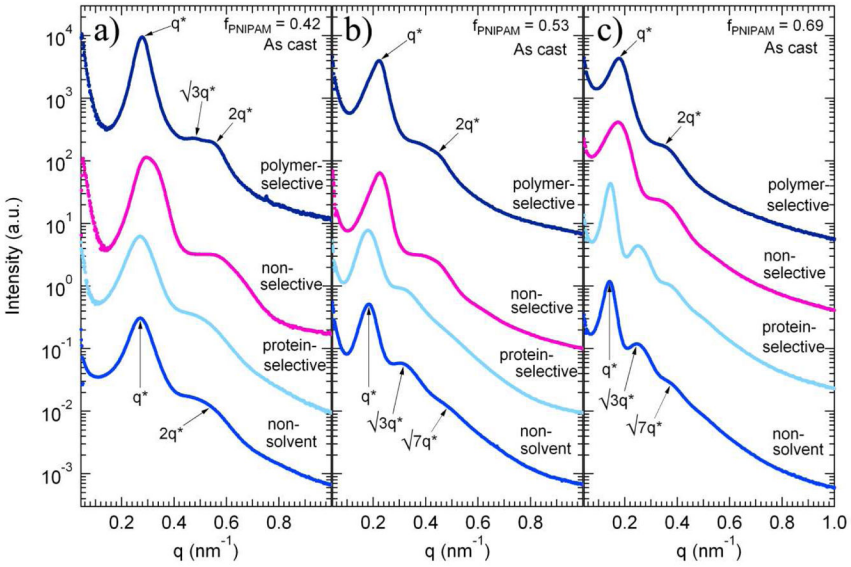

Figure 2.

Small-angle x-ray scattering data for mCherry-PNIPAM block copolymers cast from each of the four solvent types for three different PNIPAM coil fractions a) f_{PNIPAM} = 0.42 b) f_{PNIPAM} = 0.53 c) f_{PNIPAM} = 0.69. Both the coil fraction and casting condition have a significant impact on the type of nanostructure formed. The traces have been offset for clarity.

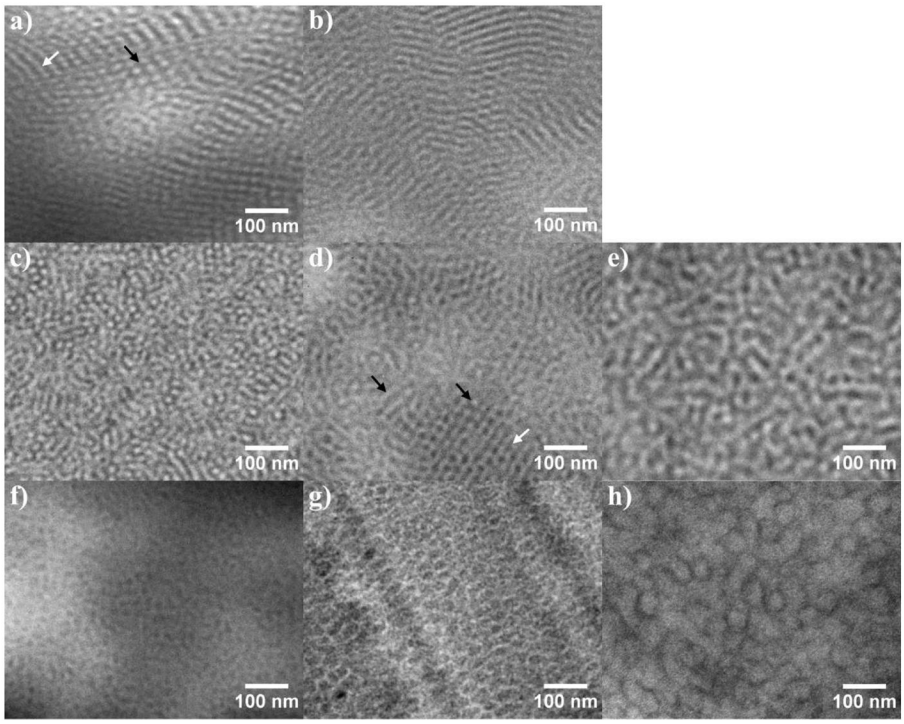

Figure 3.

TEM images for as-cast mCherry-PNIPAM block copolymers. a) cylinders cast from a polymer-selective solvent, f_{PNIPAM} = 0.42 The white arrow shows an example of cylinders parallel to the field of view, and the black arrow points out perpendicular cylinders. b) lamellae cast from a polymer-selective solvent, f_{PNIPAM} = 0.53 c) cylinders cast from a non-selective solvent, f_{PNIPAM} = 0.42 d) nanostructure cast from a non-selective solvent, f_{PNIPAM} = 0.53 The white arrow designates a region of perforated lamellae, and the black arrows show side-on and edge-on cylindrical nanostructures. e) disordered lamellae cast from a non-selective solvent, f_{PNIPAM} = 0.69 f) disordered micelles cast from a protein-selective solvent, f_{PNIPAM} = 0.42 g) hexagonally packed micelles cast from a protein-selective solvent, f_{PNIPAM} = 0.53 h) hexagonally packed micelles cast from a protein-selective solvent, f_{PNIPAM} = 0.69.

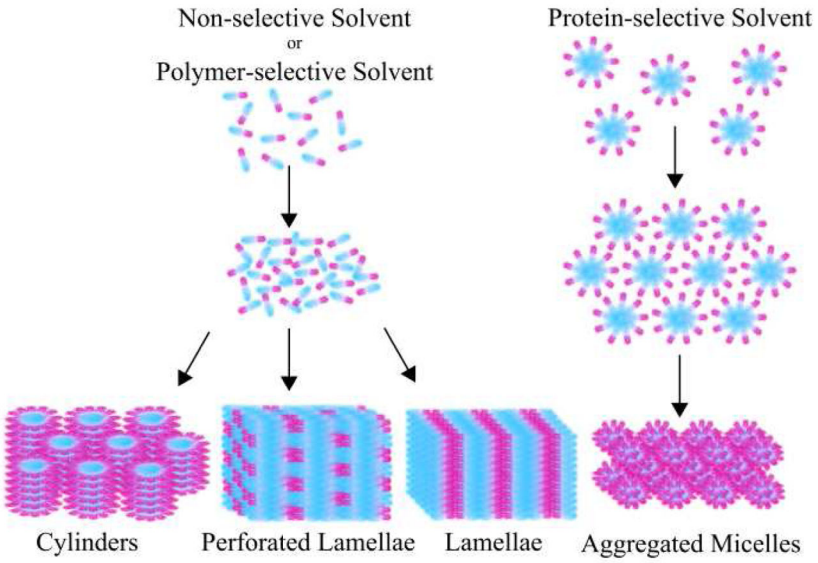

Figure 4.

Schematic depicting two observed pathways towards the self-assembly of protein-polymer block copolymers. The first occurs in a good solvent for the polymer block and results in a variety of morphologies depending on the polymer coil fraction. The second is obtained by using a poor solvent for the polymer block in which micelles are formed and subsequently aggregate into nanostructures.

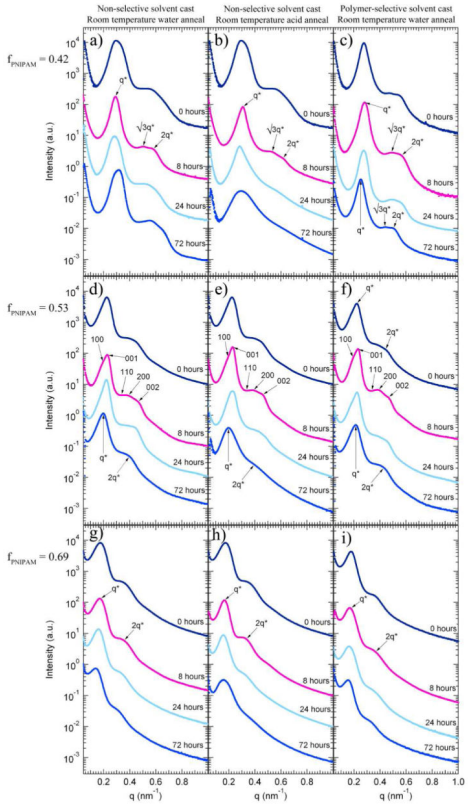

Figure 5.

Small-angle x-ray scattering data for mCherry-PNIPAM block copolymers showing the effect of solvent annealing. a–c) $f_{PNIPAM} = 0.42$ shows improved hexagonal ordering with annealing. d–f) $f_{PNIPAM} = 0.53$ shows enhancement of higher order peaks when annealing for 8 and 24 hours, indicating improved long-range ordering. Longer annealing times diminish the prominence of the higher order peaks as a result of decreased ordering. A transition in morphology from perforated lamellae to lamellae is observed with increased annealing time. g–i) $f_{PNIPAM} = 0.69$ shows slight loss of ordering with increasing annealing time.

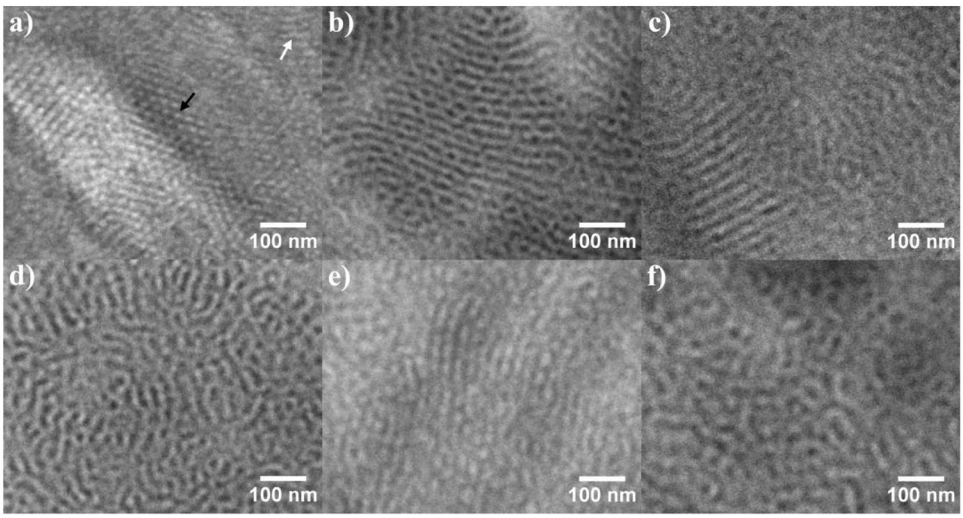

Figure 6.

TEM images for mCherry-PNIPAM block copolymers which have been solvent annealed. a) hexagonally packed cylinders from a non-selective solvent cast/water anneal for 24 hours, $f_{PNIPAM} = 0.42$ The white arrow indicates a region of edge-on cylinders, and the black arrow shows end-on cylinders. b) perforated lamellae from a polymer-selective solvent cast/water anneal for 24 hours, $f_{PNIPAM} = 0.53$ c) lamellae from a non-selective cast/water anneal for 72 hours, $f_{PNIPAM} = 0.53$ d) disordered lamellae from a non-selective solvent cast/water anneal for 24 hours, $f_{PNIPAM} = 0.53$ e) perforated lamellae from a non-selective cast/1 volume % formic acid anneal for 24 hours, $f_{PNIPAM} = 0.53$ f) disordered lamellae from a non-selective solvent cast/water anneal for 24 hours, $f_{PNIPAM} = 0.69$.

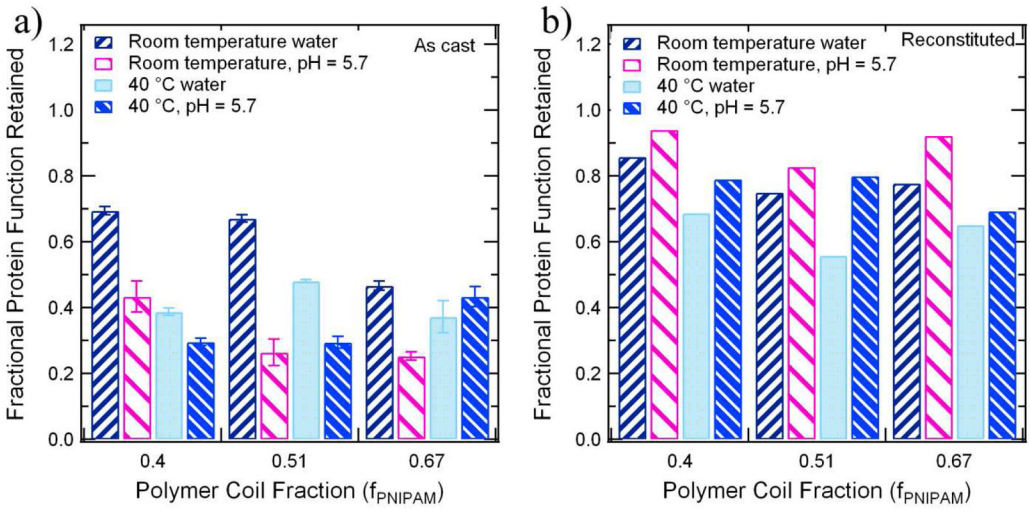

Figure 7.

Protein optical activity as a function of PNIPAM coil fraction and casting solvent. Protein function is shown in terms of the absorbance of the fluorescent protein chromophore at 586 nm, relative to the initial solution-state absorbance of the protein-polymer conjugate. Solid-state samples (a) provide a direct measure of function in solid nanostructures, while rehydrated samples (b) provide a measure of the fraction of protein that remained folded. Room temperature water is a non-selective solvent, room temperature pH = 5.7 is a polymer-selective solvent, 40 °C water is a protein-selective solvent, and 40 °C pH = 5.7 is a non-solvent for this system.

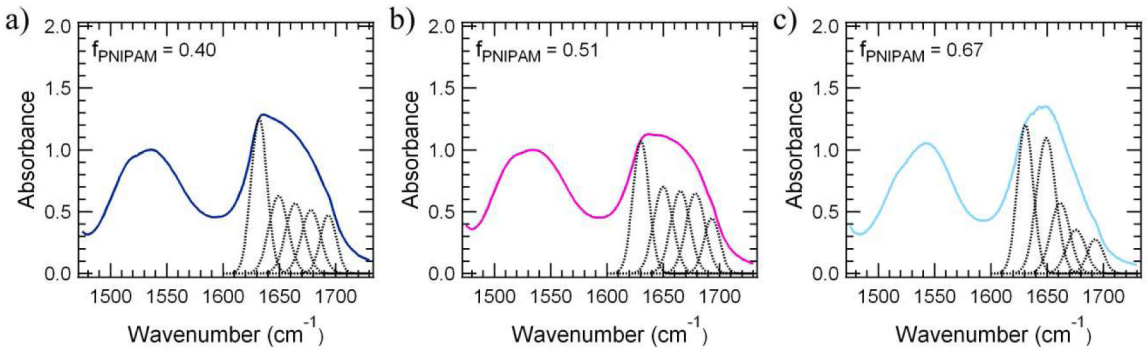

Figure 8.

Representative solid-state FTIR spectra for a) f_{PNIPAM} = 0.42 b) f_{PNIPAM} = 0.53 and c) f_{PNIPAM} = 0.69, showing the amide I region with Fourier Self-Deconvolution (FSD) overlaid. The amide I peak has greater intensity near 1631 cm^{-1} for lower PNIPAM coil fractions which indicates a predominately β-sheet structure, while for the highest PNIPAM coil fraction, the peak intensity shifts to 1649 cm^{-1}, indicating an increase in the amount of random coil content.

Table 1

mCherry-b-PNIPAM block copolymers

block copolymer	PNIPAM M_n (kg/mol)	PDI_{PNIPAM}	Conjugate M_n (kg/mol)	f_{PNIPAM}
mCherry-PNIPAM19	18.8	1.08	46.9	0.42
mCherry-PNIPAM29	29.0	1.10	57.1	0.53
mCherry-PNIPAM57	57.3	1.12	85.4	0.69

Table 2

Dynamic light scattering from 1 wt% mCherry-PNIPAM solutions

Sample	Temperature (°C)	pH	Average radius (nm) f_{PNIPAM} = 0.42 (PDI)	Average radius (nm) f_{PNIPAM} = 0.53 (PDI)	Average radius (nm) f_{PNIPAM} = 0.69 (PDI)
non-selective	25	7.5	7.3 (17%)	8.0 (24%)	11.0 (25%)
protein-selective	40	7.5	> 800 (21%)	> 800 (9%)	> 800 (27%)
polymer-selective	25	5.75	7.9 (32%)	8.2 (28%)	9.6 (22%)
non-solvent	40	5.75	> 800 (9%)	> 800 (64%)	> 800 (51%)

Table 3

FTIR peak identification according to literature

wavenumber range (cm^{-1})	peak assignment
1612–1640	beta-sheet (strong)
1640–1657	random coils
1650–1660	alpha helix
1661–1680	beta turns, loops
1681–1695	beta-sheet (weak)